Mon. Not. R. Astron. Soc. **369,** 835–845 (2006) doi:10.1111/j.1365-2966.2006.10337.x

Determination of the profile of atmospheric optical turbulence strength from SLODAR data

T. Butterley,[1] R. W. Wilson[1⋆] and M. Sarazin[2]

[1]*Department of Physics, Centre for Advanced Instrumentation, University of Durham, South Road, Durham DH1 3LE*
[2]*European Southern Observatory, Karl-Schwarzschild-Strasse 2, D-85748 Garching, Germany*

Accepted 2006 March 15. Received 2006 March 16; in original form 2006 March 6

ABSTRACT

Slope Detection and Ranging (SLODAR) is a technique for the measurement of the vertical profile of atmospheric optical turbulence strength. Its main applications are astronomical site characterization and real-time optimization of imaging with adaptive optical correction. The turbulence profile is recovered from the cross-covariance of the slope of the optical phase aberration for a double star source, measured at the telescope with a wavefront sensor (WFS). Here, we determine the theoretical response of a SLODAR system based on a Shack–Hartmann WFS to a thin turbulent layer at a given altitude, and also as a function of the spatial power spectral index of the optical phase aberrations. Recovery of the turbulence profile via fitting of these theoretical response functions is explored. The limiting resolution in altitude of the instrument and the statistical uncertainty of the measured profiles are discussed. We examine the measurement of the total integrated turbulence strength (the seeing) from the WFS data and, by subtraction, the fractional contribution from all turbulence above the maximum altitude for direct sensing of the instrument. We take into account the effects of noise in the measurement of wavefront slopes from centroids and the form of the spatial structure function of the atmospheric optical aberrations.

Key words: atmospheric effects – instrumentation: adaptive optics – site testing.

1 INTRODUCTION

An accurate knowledge of the vertical profile of the strength of atmospheric optical turbulence is critical for the optimization of adaptive optics (AO) for astronomy. Statistical profile data are required for the planning and design of next-generation AO systems for existing telescopes and for extremely large telescopes (Ellerbroek & Rigaut 2000; Le Louarn & Hubin 2004; Tokovinin 2004). Profile data available in real time can be used to optimize system parameters including servo-loop bandwidths and wavefront reconstruction algorithms (Tokovinin et al. 2001). Furthermore, contemporaneous measurements of the turbulence profile can be used to characterize anisoplanatic variations of the point spread function for de-convolution of AO-corrected images (Wilson & Jenkins 1996; Fusco et al. 2000).

Slope Detection and Ranging (SLODAR) (Wilson 2002) is an optical triangulation method for the measurement of the atmospheric optical turbulence profile $C_n^2(h)$. The method can also be used to determine the temporal characteristics and translational (wind-blown) velocity of the turbulence as a function of altitude, but in this paper we concentrate on the method for estimation of the profile of turbulence strength. The profile is determined from the spatial covariance of the slope of the wavefront phase aberration at the ground for the two distinct paths through the atmosphere defined by a double star target. The aberrations are measured using one or more wavefront sensors (WFSs).

SLODAR was first used to measure turbulence profiles using large astronomical telescopes at the Observatorio del Roque de los Muchachos, La Palma. More recently, the technique was used to implement a portable, stand-alone, turbulence profiler for European Southern Observatory (ESO), based on a 40-cm telescope (Wilson et al. 2004). In these implementations, a single Shack–Hartmann (SH) WFS is used, with a field of view large enough to permit simultaneous observations of the resulting spot patterns for both components of the double star on the same detector.

In the original analysis, the normalized turbulence profile was recovered from the measured centroid cross-covariance functions via a simple de-convolution, with the auto-covariance (measured for the brighter of the two stars) used as the impulse response of the system to a thin turbulent layer. This simple de-convolution method is inaccurate. The average centroid motion (over all subapertures in the SH array) must be subtracted from the data in order to avoid bias by the effects of telescope guiding errors and wind-shake. However, this process also removes the common tilt motion induced by the

⋆E-mail: r.w.wilson@durham.ac.uk

atmosphere itself. In the cross-covariance, this introduces a small anisoplanatic component, so that the impulse response varies slowly with altitude. Here, we determine the impulse response for SLODAR as a function of the turbulence altitude, and also as a function of the spatial power spectral density of the phase fluctuations. The fractional error in determination of the turbulence strength, if the anisoplanatic effect is ignored, ranges from zero at the ground to approximately 20 per cent at the maximum profiling altitude of the system, for the case of Kolmogorov turbulence.

In Section 2, we review the SLODAR analysis and detail the method used for the calculation of the theoretical system response as a function of the altitude of a thin turbulent layer, for a given spatial spectrum of aberrations. Section 3 explores the determination of the turbulence profile via a fit to the measured cross-covariance function, including assessments of the statistical uncertainty of the measured profile and the effective resolution in altitude. In Section 4, we examine the determination of the total integrated turbulence strength from the WFS data and, by subtraction, the fractional contribution from any turbulence at altitudes greater than the maximum altitude for direct sensing from the cross-covariance. We take into account measurement noise of the centroid values and the specific form of the spatial structure function of the atmospheric optical aberrations.

2 THE THEORETICAL IMPULSE RESPONSE FOR SLOPE DETECTION AND RANGING

For SLODAR, we measure the spatial covariance of the gradient of the optical phase aberration observed at ground level. The turbulence altitude profile is found via triangulation, as shown in Fig. 1. A layer at altitude H produces a peak in the cross-covariance function at a spatial offset equal to $H\theta$. If the 'impulse response' of the system – the shape of the covariance for a thin layer at a given altitude – is known, then the turbulence profile can be recovered via a fit to the measured cross-covariance function.

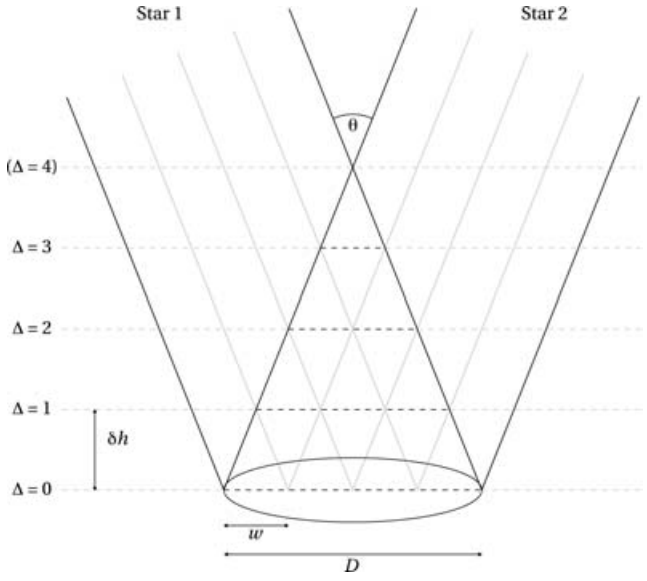

Figure 1. Overview of the SLODAR method geometry. θ is the angular separation of the double star target. D is the diameter of the telescope pupil and w the width of a single subaperture in the SH array. The centres of the sampling bins in altitude are given by $\Delta\delta h$.

The fit yields an estimate of the integrated turbulence strength in the altitude bins corresponding to each of the spatial offsets in the measured slope covariance function. The width of the bins is given by

$$\delta h = \frac{w}{\theta} \tag{1}$$

where w is the width of a WFS subaperture and θ is the angular separation of the target double star. If the WFS optics are collimated so that the lenslet array is at the optical conjugate of the telescope entrance aperture, then the point in the covariance function for zero spatial offset will correspond to a range of altitudes of width δh centred at the telescope. The remaining bins, of equal size, will be centred at altitudes $i\delta h$, $i = 1, \ldots, (N-1)$ where N is the number of WFS subapertures across the telescope pupil.

Hence, the resolution in altitude of a SLODAR system is determined by the diameter of the WFS subapertures and the angular separation of the target. For a given resolution δh, the maximum altitude for direct sensing of the turbulence profile is simply δh multiplied by the number of subapertures across the WFS. Hence, for a system based on a small telescope, the lowest altitude layers may be examined in detail by choosing targets with large separations. The main application of the ESO portable SLODAR system is characterization of the ground layer turbulence, typically with a resolution of 150 m to a maximum altitude of approximately 1 km. Low-resolution ($\delta h \sim 2$ km) profiles up to high altitudes can also be measured. For a WFS with, for example, 80×80 subapertures deployed on a 8-m telescope, profiles with a resolution of 200 m could be determined to a maximum altitude of 16 km. For any SLODAR system, the total optical turbulence strength for the whole atmosphere is also measured (see Section 4). Hence, the integrated turbulence at all altitudes greater than the maximum altitude for direct sensing is determined as the difference of the total turbulence strength and the sum of the directly measured profile.

We now determine theoretical expressions for the SLODAR cross-covariance as a function of the turbulence altitude. The centroid data for the SH WFS are a measure of the slope of the wavefront over each subaperture. $s^{x[1]}_{i,j}(t)$ is the slope in the x-direction for the subaperture $[i, j]$ for the first star, where i and j index the position of a subaperture in the SH array horizontal (x) and vertical (y) directions at time t, for the first star. Similarly $s^{x[2]}_{i,j}(t)$ for the second star.

$$s^{x[1]}_{i,j} = \int \phi\left(w\boldsymbol{r}^{[1]}_{i,j}\right) F_x\left(\boldsymbol{r}^{[1]}_{i,j}\right) W\left(\boldsymbol{r}^{[1]}_{i,j}\right) \mathrm{d}\boldsymbol{r}^{[1]}_{i,j} \tag{2}$$

where $\boldsymbol{r}^{[1]}_{i,j}$ is a spatial coordinate, defined in units of the subaperture width w, with its origin at the centre of subaperture $[i, j]$ for star 1 (similarly $\boldsymbol{r}^{[2]}_{i',j'}$ for subaperture $[i', j']$, star 2). $\phi(w\boldsymbol{r}^{[1]}_{i,j})$ is the optical phase in the plane of the aperture. $W(\boldsymbol{r})$ is the subaperture pupil function:

$$\begin{aligned} W(\boldsymbol{r}) &= 1 \text{ for } |x|, |y| < 1/2 \\ &= 0 \text{ otherwise,} \end{aligned} \tag{3}$$

and F_x is the linear slope function in the relevant direction, normalized such that

$$\int F_x^2(\boldsymbol{r}) W(\boldsymbol{r})\, \mathrm{d}\boldsymbol{r} = 1. \tag{4}$$

The cross-covariance of the slopes for two subapertures is

$$C^x_{i,j,i',j'} = \left\langle s^{x[1]}_{i,j} s^{x[2]}_{i',j'} \right\rangle \tag{5}$$

for the slope in the x-direction between subapertures $[i, j]$ for star 1 and $[i', j']$ for star 2. Similarly for the y direction. The spatial offset between the subapertures in units of w is $(\delta i, \delta j) = (i' - i,\ j' - j)$. The angular brackets denote averaging over a large number of independent realizations of the turbulent distortions over the telescope. If the orientation of the double star target is assumed to be aligned along the axis of the WFS in the x-direction, then we can consider covariance functions for the tilts in the directions longitudinal (L) and transverse (T) to the spatial offset. The L covariance for a pair of subapertures is given by

$$C^{x}_{i,j,i',j'} = \int\int \left\langle \phi^{[1]}_{i,j}\left(w\boldsymbol{r}^{[1]}_{i,j}\right)\phi^{[2]}_{i',j'}\left(w\boldsymbol{r}^{[2]}_{i',j'}\right)\right\rangle F_x\left(\boldsymbol{r}^{[1]}_{i,j}\right)F_x\left(\boldsymbol{r}^{[2]}_{i',j'}\right) \times W\left(\boldsymbol{r}^{[1]}_{i,j}\right)W\left(\boldsymbol{r}^{[2]}_{i',j'}\right)\mathrm{d}\boldsymbol{r}^{[1]}_{i,j}\mathrm{d}\boldsymbol{r}^{[2]}_{i',j'}. \quad (6)$$

The mean phase over the whole of the telescope aperture (the 'piston' term) does not affect the measurement of wavefront slopes. We therefore express the integral in terms of the covariance of the phases *relative to the aperture means*. Divergence of the calculation resulting from the pole at the origin of the spatial power spectra of the phase aberrations is then avoided. The covariance of the slopes across two subapertures can be found via a numerical integral involving the spatial structure function, $D_\phi(w\boldsymbol{x})$, of the phase aberrations (Wilson & Jenkins 1996):

$$\begin{aligned}\left\langle \Phi^{[1]}_{i,j}\left(w\boldsymbol{r}^{[1]}_{i,j}\right)\Phi^{[2]}_{i',j'}\left(w\boldsymbol{r}^{[2]}_{i',j'}\right)\right\rangle &= -\frac{1}{2}D_\phi(w\boldsymbol{x}) \\ &+ \frac{1}{2}\int W\left(\boldsymbol{r}^{[1]}_{i,j}\right)D_\phi(w\boldsymbol{x})\,\mathrm{d}\boldsymbol{r}^{[1]}_{i,j} \\ &+ \frac{1}{2}\int W\left(\boldsymbol{r}^{[2]}_{i',j'}\right)D_\phi(w\boldsymbol{x})\,\mathrm{d}\boldsymbol{r}^{[2]}_{i',j'} \\ &- \frac{1}{2}\int\int W\left(\boldsymbol{r}^{[1]}_{i,j}\right)W\left(\boldsymbol{r}^{[2]}_{i',j'}\right)D_\phi(w\boldsymbol{x})\,\mathrm{d}\boldsymbol{r}^{[1]}_{i,j}\mathrm{d}\boldsymbol{r}^{[2]}_{i',j'}, \end{aligned} \quad (7)$$

where $\Phi^{[1]}_{i,j}\left(w\boldsymbol{r}^{[1]}_{i,j}\right)$ is the phase relative to the aperture mean,

$$\boldsymbol{x} = \boldsymbol{u} + \boldsymbol{r}^{[2]}_{i',j'} - \boldsymbol{r}^{[1]}_{i,j} \quad (8)$$

and $\boldsymbol{u}$ is the vector separation of the subapertures in units of the subaperture width w (see Fig. 2), and is given by

$$\boldsymbol{u} = (i' - i + \Delta,\ j' - j). \quad (9)$$

To remove the effect of common motions induced by telescope guiding errors and wind-shake, we subtract the mean slope for all subapertures from the instantaneous slopes at each subaperture. The global tilt subtraction is carried out separately for stars 1 and 2. This introduces a dependence of the subaperture covariances on the altitude of the turbulence. For a turbulent layer at an altitude H, corresponding to an offset of $\Delta = H\theta/w$ in the x-direction (in units of w) between the projections of the telescope pupil on to the turbulent layer for the two stars, the covariance of the slopes for two subapertures after global tilt subtraction, is

$$\begin{aligned}C'^{x}_{i,j,i',j'}(\Delta) &= \left\langle \left(s^{[1]}_{i,j} - \overline{s^{[1]}}\right)\left(s^{[2]}_{i'+\Delta,j'} - \overline{s^{[2]}}\right)\right\rangle \\ &= \left\langle s^{[1]}_{i,j}s^{[2]}_{i'+\Delta,j'}\right\rangle - \left\langle s^{[1]}_{i,j}\overline{s^{[2]}}\right\rangle \\ &\quad - \left\langle \overline{s^{[1]}}s^{[2]}_{i'+\Delta,j'}\right\rangle + \left\langle \overline{s^{[1]}}\,\overline{s^{[2]}}\right\rangle \end{aligned} \quad (10)$$

where $\overline{s^{[1]}}$ is the slope for star 1 averaged over all subapertures, for example,

$$\overline{s^{[1]}} = \frac{1}{N_{\mathrm{sub}}}\sum_{\text{valid } i,j} s^{[1]}_{i,j} \quad (11)$$

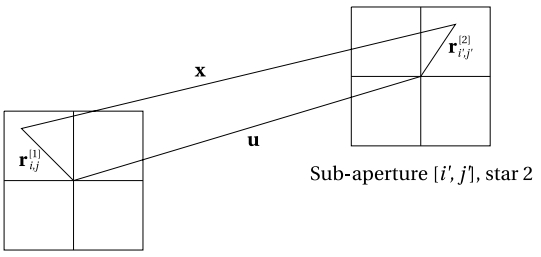

Figure 2. Geometry for the calculation of the covariance of wavefront slopes across WFS subapertures.

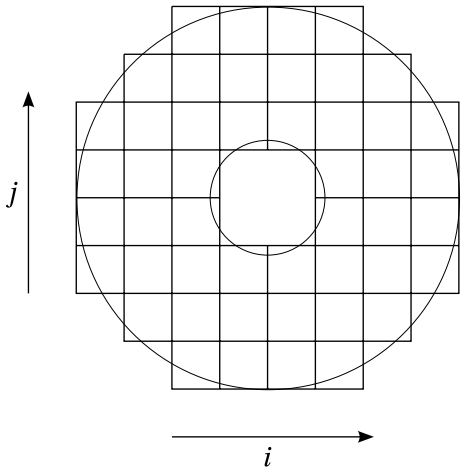

Figure 3. Pupil geometry for the 8 × 8 subaperture ESO portable SLODAR system, showing the mapping of the square WFS subapertures on to the annular aperture function of the Meade LX200 telescope.

$$\left\langle \overline{s^{[1]}}s^{[2]}_{i'+\Delta,j'}\right\rangle = \frac{1}{N_{\mathrm{sub}}}\sum_{\text{valid } i,j}\left\langle s^{[1]}_{i,j}s^{[2]}_{i'+\Delta,j'}\right\rangle \quad (12)$$

where N_{sub} is the total number of subapertures and 'valid i, j' indicates all values of i and j for which the corresponding subaperture is not vignetted (dependent on WFS/pupil geometry, for example, see Fig. 3).

For SLODAR, we average over all overlapping subaperture pairs for a given spatial separation $(\delta i, \delta j)$, taking into account the projection of the telescope pupil function on to the subaperture array. The response of SLODAR to a turbulent layer at altitude H is therefore described by

$$X_{\mathrm{L}}(\Delta, \delta i, \delta j) = \frac{1}{N_{\mathrm{cross}}}\sum_{\text{valid } i,j,i',j'} C'^{x}_{i,j,i',j'}(\Delta) \quad (13)$$

where valid $i,\ j,\ i',\ j'$ refers to all values of i, j, i' and j' such that subapertures $[i, j]$ and $[i', j']$ both exist, remembering that $(i',\ j') = (i + \delta i,\ j + \delta j)$. N_{cross} is the number of such existing subaperture pairs for a given $(\delta i, \delta j)$.

The impulse response functions are two dimensional. However, two-dimensional information is only required if the velocities of the turbulent layers are to be measured. Velocity information can be obtained by introducing a temporal offset between the centroid

data being correlated for the two stars and observing the resulting spatial offset of the peaks in the two-dimensional cross-covariance function. If only the turbulence strength as a function of altitude is required, all of the necessary information is contained in a cut through the two-dimensional covariance function in the x-direction, at $y = 0$. Hence, we can set $j = j'$ in equation (13) to obtain a set of one-dimensional response functions:

$$X_{\mathrm{L}}(\Delta, \delta i) = \frac{1}{N_{\mathrm{cross}}} \sum_{\text{valid } i,j,i'} C'^{x}_{i,j,i',j}(\Delta). \tag{14}$$

The shape of the slope covariance function depends on the underlying power law describing the spatial fluctuations of the phase. For the standard Kolmogorov model of atmospheric turbulence, the spatial spectrum of aberrations at the ground follows a power law with exponent $-11/3$. Here, we also explore two alternative models for the spatial power spectrum – the von Karman spectrum and the generalized spectrum.

The von Karman spectrum again assumes an underlying spectrum with slope $-11/3$, but the spectrum is modified to take into account the finite spatial outer scale of aberrations:

$$I_{\phi}(\kappa) = 0.022\,883 r_0^{-5/3} \frac{L_0^{11/3}}{\left(1 + L_0^2 \kappa^2\right)^{11/6}}, \tag{15}$$

where κ is the spatial frequency modulus, r_0 is the Fried parameter and L_0 is the outer scale. The corresponding form for the spatial structure function of the phase is (Jenkins 1998)

$$D_{\phi}(r) = 0.172\,53 \left(\frac{L_0}{r_0}\right)^{5/3} \times \left[1 - \frac{2\pi^{5/6}}{\Gamma(5/6)} \left(\frac{r}{L_0}\right)^{5/6} K_{5/6}\left(2\pi \frac{r}{L_0}\right)\right], \tag{16}$$

where K is a modified Bessel function of the second kind.

A generalized expression for the phase spectrum was described by Nicholls, Boreman & Dainty (1995):

$$I_{\phi}(\kappa) = \frac{A_{\beta} \kappa^{-\beta}}{\rho_0^{\beta-2}} (2 < \beta < 4), \tag{17}$$

where ρ_0 is analogous to r_0 in Kolmogorov turbulence and the constant A_{β} is chosen such that the piston-subtracted wavefront variance over a pupil diameter $D = \rho_0$ is equal to 1 rad^2. Note that this differs slightly from the Kolmogorov definition so that a generalized power spectrum with $\beta = 11/3$ matches the Kolmogorov form when $\rho_0 = 0.982\, r_0$. The value of A_{β} is given by (Boreman & Dainty 1996):

$$A_{\beta} = \frac{2^{\beta-2}\left[\Gamma\left(\frac{\beta+2}{2}\right)\right]^2 \Gamma\left(\frac{\beta+4}{2}\right) \Gamma\left(\frac{\beta}{2}\right) \sin\left(\pi \frac{\beta-2}{2}\right)}{\pi^{\beta} \Gamma(\beta+1)}. \tag{18}$$

The corresponding form for the phase structure function is

$$D_{\phi}(r) = \gamma_{\beta} \left(\frac{r}{\rho_0}\right)^{\beta-2} \tag{19}$$

where γ_{β} is a constant that keeps consistency between the power spectrum and the structure function, given by Rao, Jiang & Ling (2000):

$$\gamma_{\beta} = \frac{2^{\beta-1}\left[\Gamma\left(\frac{\beta+2}{2}\right)\right]^2 \Gamma\left(\frac{\beta+4}{2}\right)}{\Gamma\left(\frac{\beta}{2}\right) \Gamma(\beta+1)}. \tag{20}$$

For a given WFS and telescope pupil geometry, the individual subaperture tilt covariances (with global tilt correction) can now be calculated from equations (6) and (7) via numerical integration. The SLODAR impulse response functions are then found from equation (14) by averaging over all overlapping subaperture pairs for each offset δi.

Figs 4 and 5 plot the resulting normalized impulse response functions for the case of the 8×8 subaperture system with the geometry shown in Fig. 3. The ratio of the telescope aperture size to the diameter of central obscuration in this case is identical to that for the 40-cm Meade LX200 telescope employed for the ESO portable SLODAR system. The shape of the response functions for this case will be correct for any system with same WFS/pupil geometry, regardless of the telescope aperture size. Subapertures that are less than 70 per cent illuminated are excluded from the analysis. In Fig. 4, we plot the longitudinal and transverse response functions for the von Karman power spectrum with $L_0 = 1$, 2 and 10 times the telescope aperture diameter. In Fig. 5, we plot the response functions for the generalized power spectrum with $\beta = 9/3$, $10/3$ and $11/3$. In each plot, the response functions are normalized to the value of the covariance for $\delta i = 0$ and $\Delta = 0$.

For the von Karman spectrum and a given value of L_0, the impulse response functions scale as $r_0^{-5/3}$. For the generalized spectrum, they scale as $\rho_0^{2-\beta}$.

We note that equation (2) strictly refers to the Zernike tilt ('Z-tilt') of the wavefront across the subaperture. This differs slightly from the mean or gradient tilt ('G-tilt') of the wavefront (see e.g. Tokovinin 2002). The actual gradient measured will be closer to the Z-tilt or G-tilt depending on the details of the image-centring algorithm used. The classical centroid, or centre of mass, yields the G-tilt. However, if the images are strongly thresholded or are fitted to a Gaussian, then the measured tilt will be closer to the Z-tilt. A Monte Carlo simulation of the SLODAR WFS, based on translating random phase screens with the required spatial structure function of aberrations, was used to provide an independent check on the form of the impulse response functions and to investigate any possible effect resulting from the details of the centroiding algorithm. The centroiding algorithm employed in the simulation was identical to that used for analysis of real SLODAR data. A threshold was applied to the image data before calculation of the centre of mass to remove the influence of detector read-out noise on the centroids. The results for the simulation matched the numerical results shown in Figs 4 and 5 to within the statistical uncertainty of the simulation approach.

From Figs 4 and 5, we note that the width of the covariance function in the longitudinal direction drops more rapidly with increasing spatial offset than for the transverse direction. Furthermore, the difference between the L and T functions increases as the outer scale decreases or as the power-law coefficient β decreases – as we deviate from the Kolmogorov case, the width of the longitudinal functions decreases more rapidly than for the transverse functions. Similar sets of covariance functions can be produced for the von Karman and generalized spectra by adjusting the values of β and L_0. Hence, in practice, it may be difficult to distinguish which of the two models is more applicable.

The calculated impulse response functions are for the high light level case (zero centroid measurement noise). Centroiding noise resulting from shot noise and detector read-out noise in the WFS images will produce a small, but not always negligible, bias of the measured cross-covariance. Before subtraction of the mean slope, the cross-covariance functions are not biased by shot noise, since the noise is statistically independent for different subapertures and reference stars. Subtracting the mean tilt adds a constant bias to the cross-covariance, equal to the centroid noise variance for a

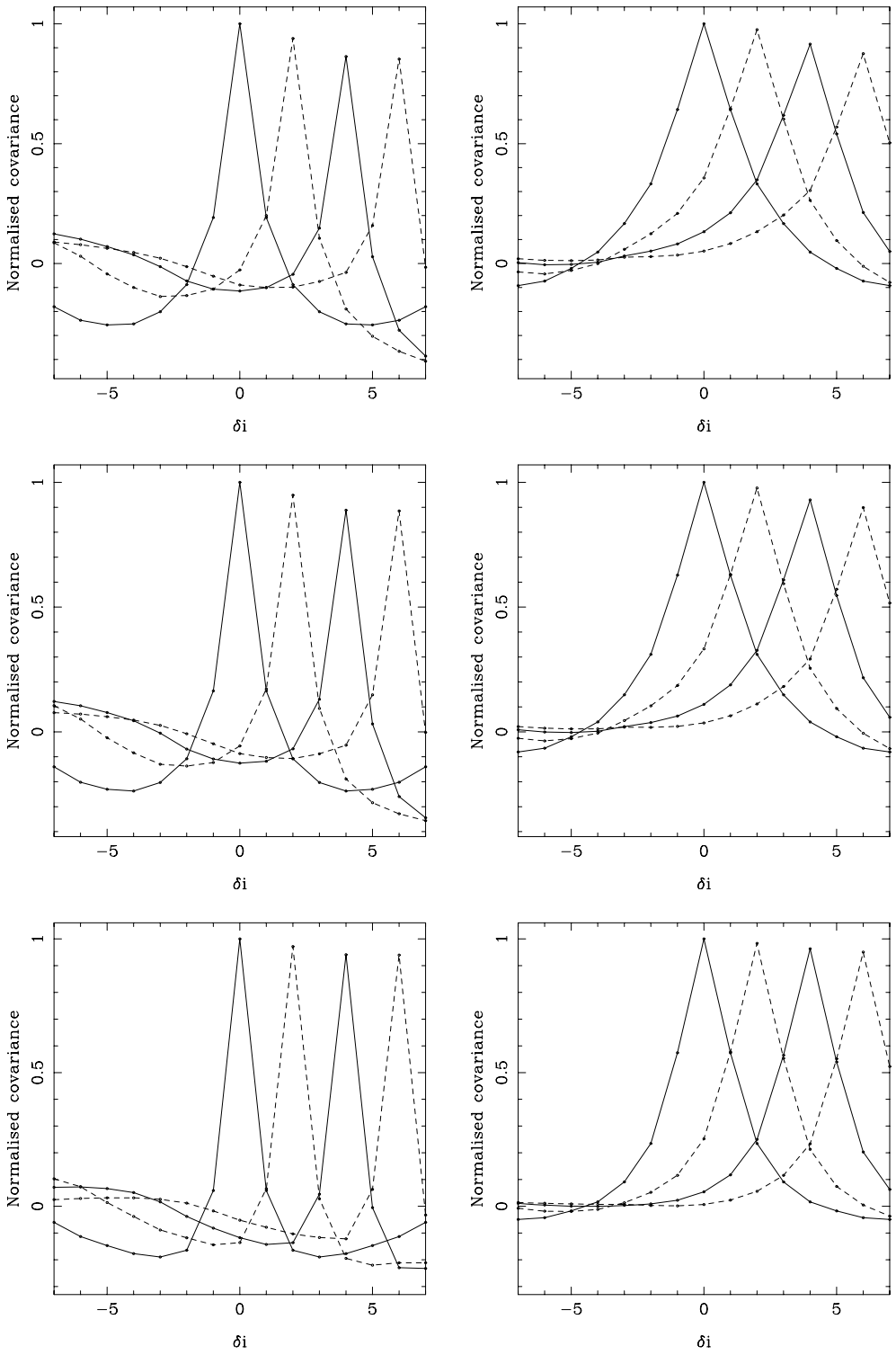

Figure 4. Normalized SLODAR theoretical impulse response functions for the von Karman spectrum of turbulence and the 8 × 8 WFS geometry shown in Fig. 3. The left-hand panel: longitudinal (L), the right-hand panel: transverse (T) covariance. From the top to bottom panel, $L_0 = 10$, 2 and 1 times the telescope aperture diameter. Each plot shows response functions for $\Delta = 0$ (peak at $\delta i = 0$), 2, 4 and 6, corresponding to increasing layer altitudes above the telescope. In each panel, the covariance values are normalized relative to the value for $\delta i = 0$ and $\Delta = 0$.

single subaperture divided by the number of valid subapertures in the WFS array. In typical conditions, the noise variance is of the order 10 per cent of the total centroid variance, so that the bias on the cross-covariance is ∼0.2 per cent of the total centroid variance for the Meade-based SLODAR system. The centroid noise variance and, hence, the cross-covariance bias level can be estimated from the shape of the auto-covariance function (see Section 4).

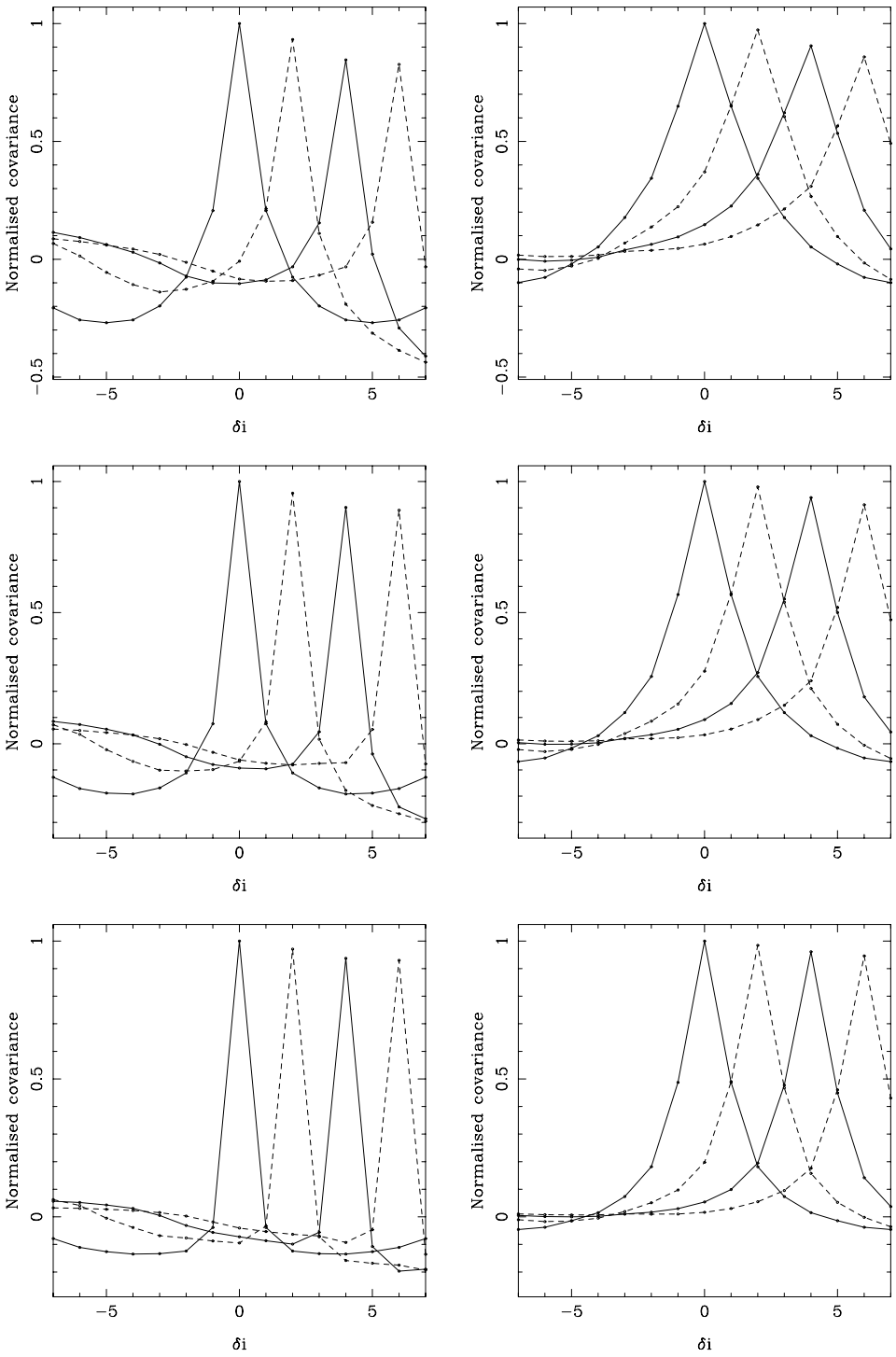

Figure 5. Normalized SLODAR theoretical impulse response functions for generalized spectrum, for the WFS geometry shown in Fig. 3. The left-hand panel: longitudinal (L), the right-hand panel: transverse (T) covariance. From the top to bottom panel, $\beta = 11/3$, $10/3$ and $9/3$. Each plot shows response functions for $\Delta = 0$ (peak at $\delta i = 0$), 2, 4 and 6, corresponding to increasing layer altitudes above the telescope. In each panel, the covariance values are normalized relative to the value for $\delta i = 0$ and $\Delta = 0$.

3 ESTIMATION OF THE TURBULENCE PROFILE

3.1 Profile fitting

A measure of the vertical profile of atmospheric turbulence can now be found by fitting the altitude-dependent impulse response functions to the measured tilt covariance values. The impulse response functions are close to orthogonal so that the generalized inverse of the response function matrix can be used to obtain the profile by multiplication with the cross-covariance.

In practice, the fit may be more complicated if the spatial spectrum of the phase aberrations varies significantly with altitude. Here, we

consider the generalized spectrum where the value of β may vary with altitude. A similar argument applies to the von Karman spectrum if L_0 is not constant with altitude.

For example, in an individual case, a global best fit over all altitudes might be found using the impulse response functions for $\beta = 11/3$. However, if an individual turbulent layer (e.g. the surface layer) is in reality characterized by a smaller value of β, then spurious and unphysical negative values ('side-lobes') may appear in the profile estimate adjacent to the layer, since the model response functions will be too broad. Conversely, if we assume a global value for β that is smaller than the actual value for an individual layer, then we will effectively lose resolution in the restored profile for that layer – the impulse response functions are too narrow, so that the some of the signal due to a layer centred at one resolution element will be 'smeared' into neighbouring elements.

For a SLODAR WFS system with high spatial sampling (e.g. 30×30 subapertures across a large telescope), it would be theoretically possible to measure both the turbulence strength and β as a function of altitude. Where individual layers were clearly separated in altitude, a value of β could be found for each by fitting to the shape of individual peaks in the two-dimensional covariance function. For the low-resolution (8×8) portable SLODAR system, there is insufficient spatial resolution to apply this method. We therefore assume that the value of β is the same for all altitudes and seek the best fit to the data (in the least-squares sense) as a function of β. However, we bear in mind that the appearance of persistent negative values adjacent to peaks in the fitted profiles may indicate a failure of this approach.

Examples of data recorded with the ESO portable SLODAR system (8×8 subapertures on a 40-cm telescope) and with a SLODAR system at the 4.2-m William Herschel telescope (12×12 subapertures) are shown in Fig. 6. Best-fitting curves for the auto-covariance and cross-covariance, assuming the generalized turbulence spectrum are shown. For the ESO system example, the best fit was obtained for $\beta = 3.33$. For the WHT example, the broken line shows the best fit obtained when the value of β was assumed to be the same for all altitudes, yielding a best-fitting value of $\beta = 3.45$. In this case, an improved fit could be obtained, for the same resulting turbulence profile, by reducing the value of β for the profile bin centred at zero altitude *only* to 3.25. Hence, in this case, there is evidence that the lowest-altitude turbulence (including surface-layer turbulence and any dome and mirror turbulence) is characterized by a spatial spectrum with a shallower slope than for the higher-altitude turbulence.

Error bars show the statistical uncertainties estimated by dividing each data set into 10 subsamples and measuring the resulting standard error of the scatter of the covariance and fitted turbulence profile values.

3.2 Statistical uncertainty of the measured profile

The uncertainty on the estimate of the integrated turbulence strength in each altitude bin depends on the number of independent samples contributing to the centroid covariance measurements. The distribution of covariance values for a given spatial offset is approximately normal. Hence, if we assume that the statistics of the turbulence are stationary – i.e. the underlying value of r_0 associated with each turbulent layer does not change with time – then we expect the statistical uncertainty of the covariance, and hence the turbulence profile estimate, to decrease as the square root of the number of independent samples. The observing time required to observe a given number of independent atmospheric 'realizations' of the wavefront aberration is dependent on the translational wind-speed associated with the turbulent layers. For higher wind-speeds, a shorter observing time will be required to achieve a required uncertainty in the profile measurement. Given that the wind-speed is not constant with altitude, we may also expect the statistical uncertainty of the profile to vary with altitude. For example, high-altitude wind speeds are typically much higher than those at the ground, so that characterization of the low-altitude ('ground layer') turbulence may require longer observing times than for the high-altitude ('free atmosphere') profile.

The number of independent samples contributing to each measurement of variance also depends to some degree on the number of valid overlapping subapertures $N_{\rm cross}$ for each spatial offset, and will be proportional to $\sqrt{N_{\rm cross}}$ for normally distributed data. $N_{\rm cross}$ decreases with increasing offset Δ, so that the statistical uncertainty of the profile will be somewhat greater for samples corresponding to higher altitudes.

Fig. 7 shows examples of temporal variations of the estimated profile for simulated and real data for the ESO portable SLODAR system. In the simulated example (top panel), the input atmospheric turbulence profile consisted of a single phase screen located at the telescope altitude, so that only the first, zero-altitude, sampling bin should be non-zero. The simulation assumed a translation of the turbulent layer at 10 m s^{-1} and a total sampling time of 15 s per measurement. 20 independent profile estimates are plotted to show the scatter. The broken line is the mean of the 20 resulting profile estimates.

The input phase screen was characterized by an integrated turbulence strength of $C_n^2\,{\rm d}h = 3.50 \times 10^{-13}$ m$^{1/3}$. The mean measured value of $C_n^2\,{\rm d}\,h$ in the zero-altitude bin was 3.45×10^{-13} m$^{1/3}$ with a standard error of 4×10^{-15} m$^{1/3}$. The standard error for the distributions of measured values in the remaining bins (except for the largest offset, $\Delta = 7$) was approximately 1×10^{-15} m$^{1/3}$. For these bins the mean measured values were each consistent with zero within twice the standard error. As expected, the scatter for the final bin corresponding to $\Delta = 7$ was significantly greater than for smaller offsets, with a standard error of 3×10^{-15} m$^{1/3}$.

The middle and bottom panels of Fig. 7 show the scatter for 20 successive profile measurements recorded over two example 20-min periods at Cerro Paranal on 2005 March 26 and 2005 August 4, respectively. Each individual profile was determined from a sequence of WFS data of duration 15 s. The first example of real data (middle panel) was chosen to have no significant turbulence above the first bin. As for the simulated example, the mean measured values for $\Delta > 0$ are consistent with zero, with standard errors of approximately (2×10^{-15} m$^{1/3}$). The scatter of the values for $\Delta = 0$ is large in this case, probably due to fluctuations of the strength of the surface layer turbulence on time-scales of a few minutes.

The example from 2005 August 4 (bottom panel) shows detection of a weak layer at the altitude corresponding to the 4th bin (centred at an altitude of 650 m) in addition to the stronger surface layer. This example gives a good indication of the sensitivity of the ESO SLODAR system as a function of the observing time in typical conditions – the layer at 650 m with strength 5×10^{-14} m$^{1/3}$ is detected at the 2σ level in an individual 15-s observation and at the 7σ level in a total observing sample of 300 s comprising the 20 individual 15-s samples.

3.3 Altitude resolution

As discussed in Section 2, the resolution in altitude of the SLODAR method for a given angular separation of the target double star is limited by the finite diameter of the WFS subapertures. In the absence

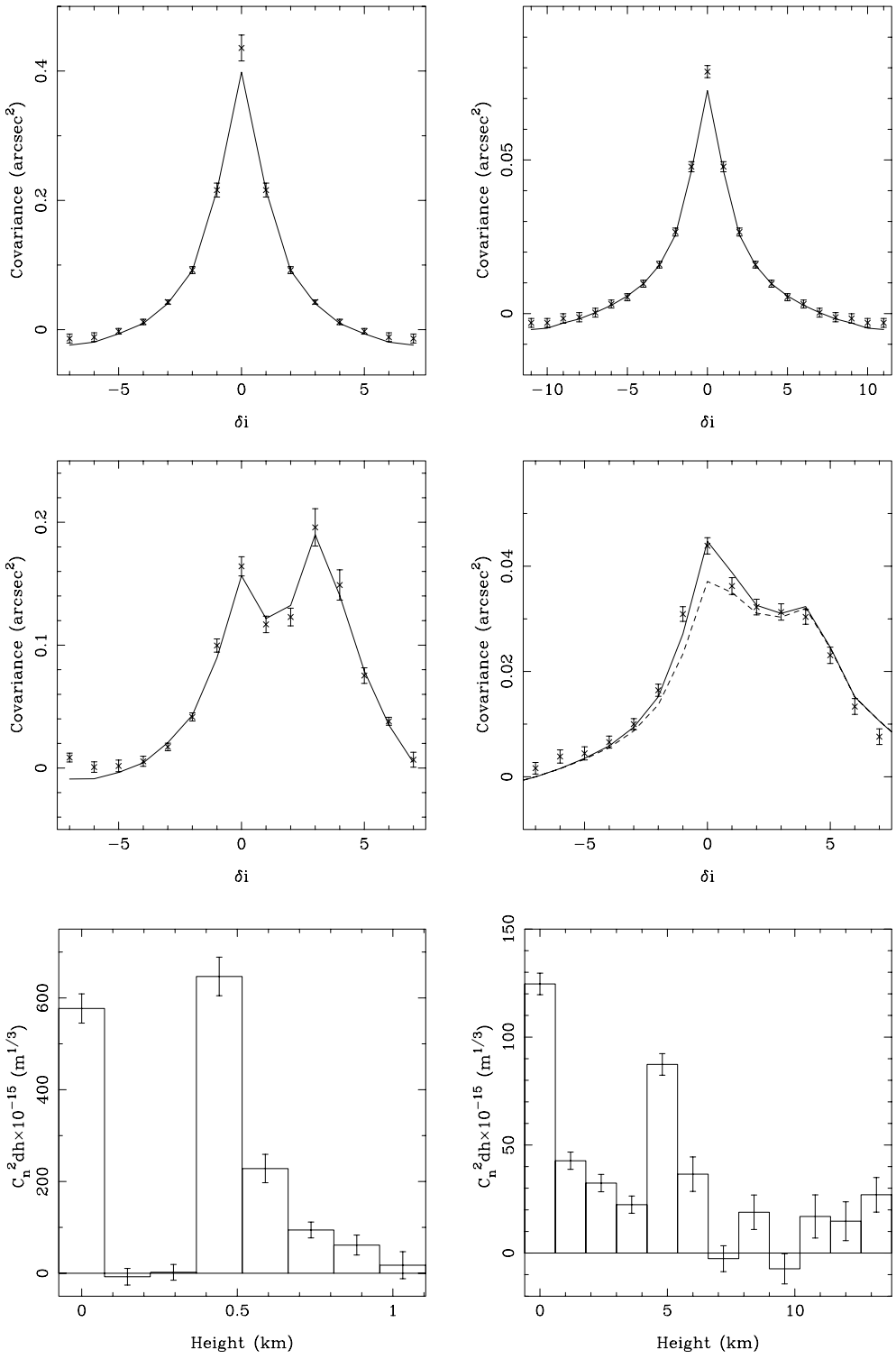

Figure 6. Example measured auto-covariance (top panels) and cross-covariance functions (middle panels) with the ESO portable SLODAR system at Cerro Paranal (left-hand panel) and a SLODAR system at the William Herschel telescope (right-hand panel). Solid and broken lines are fits of the theoretical covariance functions (see Section 3.1). The bottom panels show the optical turbulence profile estimate in each case. The data correspond to a single WFS sample sequence in each case, of duration 15 s for the ESO system and 30 s for the WHT example.

of noise on the measurements of covariance of the wavefront slopes, the measured profile will be the actual turbulence profile convolved with a rectangular function with unit area and with width δh given by equation (1). This is then sampled by the SLODAR resolution elements of width δh centred at $i\delta h$, $i = 1, \ldots, (N - 1)$, where N is the number of WFS subapertures across the telescope pupil.

Fig. 8 gives a schematic demonstration of the theoretical limit for the altitude resolution. The input turbulence profile consists of two

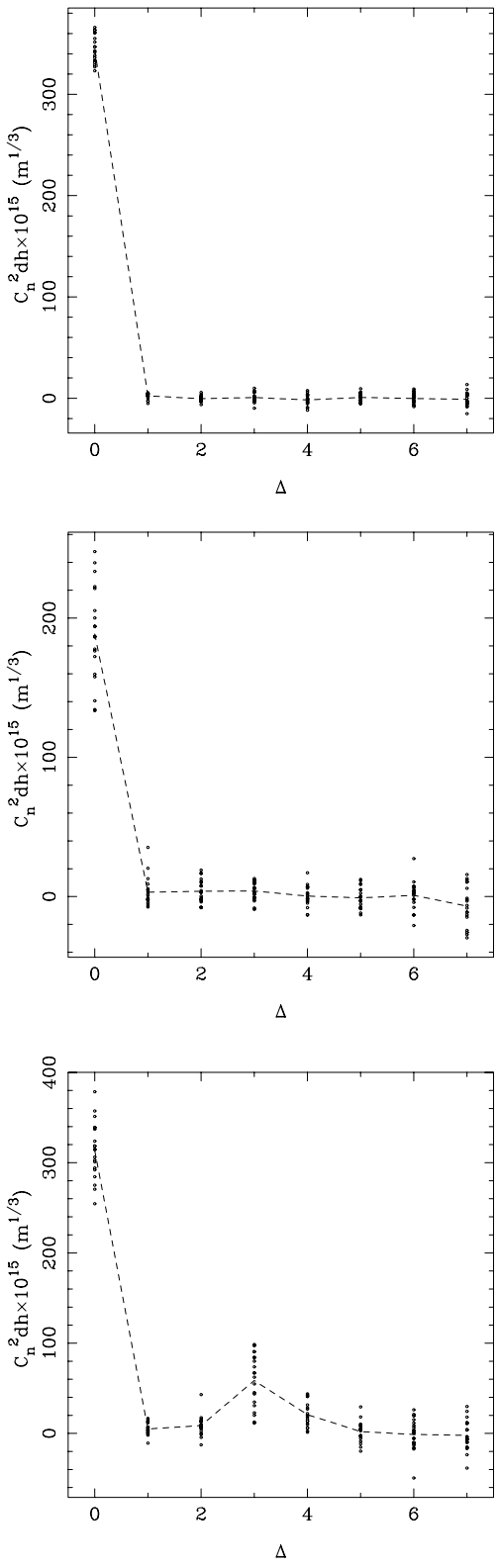

Figure 7. Examples of the statistical fluctuation of the measured turbulence profile for the ESO portable turbulence profiler (see Section 3.2). The top panel: simulated data. The middle and bottom panels: data recorded at Cerro Paranal on 2005 March 26 and 2005 August 4.

thin layers. We assume that there is no noise or statistical uncertainty on the measured cross-covariance function, so that recovery of the layer strengths and altitudes by fitting of the impulse response functions is limited only by the finite resolution in altitude of the system. Then when the altitude of a thin turbulent layer corresponds exactly to the centre of one of the SLODAR resolution bins, the recovered profile will be zero everywhere except for that bin. In all other cases, when the value of the spatial offset Δ corresponding to the altitude of the layer is not integer, we will observe non-zero turbulence strength in two adjacent resolution elements. For example, when the layer altitude corresponds to the boundary of two resolution elements, we will observe equal turbulence strength in these neighbouring bins. We note that the measured profile in this case is essentially indistinguishable from that for two half-strength layers lying at altitudes corresponding to the centres of the two adjacent bins.

In the first panel of Fig. 8, we show the recovered profile for an input turbulence profile comprising layers at altitudes corresponding to $\Delta = 3$ and 4.5 at the WFS. For this case, we observe non-zero turbulence strength in three adjacent resolution elements. From the restored profile, we could conclude that the input profile consisted of at least two thin layers, or of a single layer that was extended in altitude. In the second panel, the input profile consists of layers at altitudes corresponding to $\Delta = 3$ and 5. The measured profile is zero except for bins 3 and 5, and the two layers are fully resolved.

4 ESTIMATION OF THE TOTAL INTEGRATED TURBULENCE STRENGTH

Unless the maximum sensing altitude for direct SLODAR profiling is sufficiently high to encompass all turbulent layers, the integral of the measured turbulence profile will be less than the total turbulence strength for the whole atmosphere.

However, in all cases, the WFS data can be used to estimate the total integrated turbulence strength from all altitudes and hence – by subtraction – the summed contribution from all altitudes above the maximum sensing altitude.

In the absence of noise in the WFS images, the total turbulence strength could be determined simply from the centroid variance. When there is significant noise in the centroid measurements, the true (atmospherically induced) centroid variance can be deduced if a theoretical estimate of the noise contribution to the centroid variance is made, as a function of the target flux and detector noise characteristics. This approach is used in calibrating measurements of the integrated turbulence strength with DIMM (differential image motion) seeing monitors (Sarazin & Roddier 1990).

For SLODAR, measurement of the full slope auto-covariance function provides an alternative approach to estimation of the total turbulence strength, via a method similar to that suggested by Nicholls et al. (1995) and Rao, Jiang & Ling (2002) for the case of the generalized model. This circumvents the requirement to estimate the centroid noise variance. The same approach can be used for any other model of the spatial spectrum of the aberrations, including the von Karman model.

The shape of the tilt auto-covariance function is strongly dependent on β, particularly for longitudinal tilts. Hence, accurate estimates of both ρ_0 and β can be found via a fit to the auto-covariance function. The effects of centroid measurement noise can be avoided almost entirely by excluding the central point (zero spatial offset, the centroid variance) from the fit. Subtraction of the average slope results in a small bias of the remaining points of the auto-covariance, and the entire cross-covariance function, due to detector and shot

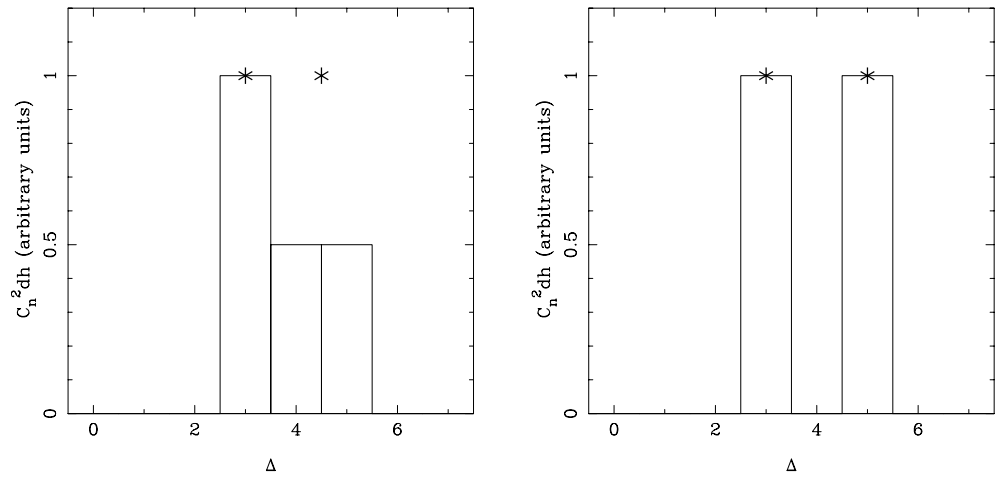

Figure 8. Schematic demonstration of the limiting resolution of the SLODAR method (see Section 3.3). Star symbols mark the spatial offsets corresponding to the altitudes of the input turbulent layers.

noise (see Section 2). However, this is negligible under normal conditions. Hence, an accurate estimate of the centroid variance due to the atmospheric aberrations in the absence of noise is given by the central value of the fitted auto-covariance function. The difference of the measured centroid variance and the atmospheric centroid variance estimated by this method yields a value for the centroid noise variance. This can be used to correct for the small noise bias level in the measured cross-covariance functions and the resulting turbulence profiles.

The noise estimation procedure is demonstrated in Fig. 9, which shows the measured and fitted transverse auto-covariance functions for simulated data as the level of noise in the centroid estimation is increased. The simulation included a single translating random-phase screen with aberrations characterized by $\rho_0 = 15$ cm and $\beta = 11/3$, and an accurate realization of the WFS in the low light level case. The theoretical intensities for each detector pixel in the WFS subaperture images were calculated for each instantaneous realization of the simulated atmosphere, for a total observation period equivalent to 15 s. The pixel values were then replaced with random deviates drawn from a Poisson distribution with mean equal to the theoretical instantaneous pixel intensity, before the image centroids were measured.

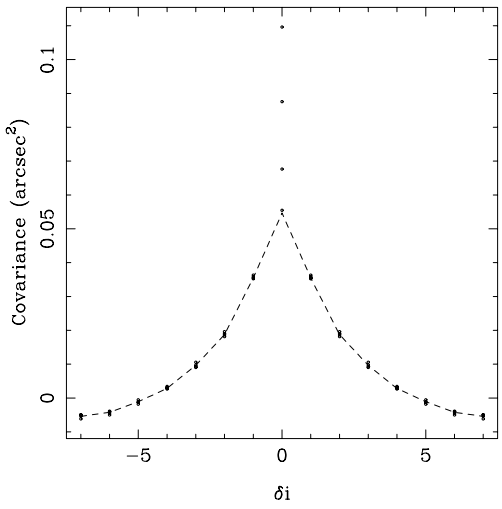

Figure 9. Demonstration of the method for estimation of the atmospheric and measurement noise contributions to the centroid variance, for simulated data (see Section 4).

The spatial auto-covariances of the measured centroids are plotted for three examples of simulated data with the same spectrum of atmospheric aberrations, but with increasing centroid noise (decreasing light level in the WFS). The theoretical auto-covariance function for the best-fitting values of ρ_0 and β is shown (broken line) for the lowest-noise case. The central value of the auto-covariance (the centroid variance itself) is excluded from the fit. The remaining points of the auto-covariance are only very weakly biased by the measurement noise (see Section 2), so that the fit is independent of the noise level in normal conditions. Hence, the turbulence and noise contributions to the centroid variance can be distinguished accurately.

5 CONCLUSIONS

The response of a SLODAR (SH) optical turbulence profiling system to a thin turbulent layer, in terms of the cross-covariance function of the wavefront slopes for a double star target, can be calculated as a function of the layer altitude and the spatial structure function of the phase aberrations. The theoretical response functions can be used to provide a robust determination of the optical turbulence profile via a fit to the covariance of the measured centroid data. The integrated turbulence strength can be calculated via a method that avoids modelling of the WFS measurement noise.

ACKNOWLEDGMENTS

We are grateful to Andrei Tokovinin for helpful comments and suggestions. The William Herschel telescope is operated on the island of La Palma by the Isaac Newton group in the Spanish Observatorio del Roque de los Muchachos of the Instituto Astrofisica de Canarias. We are grateful to the UK Particle Physics and Astronomy Research Council for financial support (TB, RWW).

REFERENCES

Boreman G. D., Dainty J. C., 1996, J. Opt. Soc. Am. A, 13, 517
Ellerbroek B. L., Rigaut F. J., 2000, Proc. SPIE, 4007, 1008
Fusco T., Conan J. M., Mugnier L. M., Michau V., Rousset G., 2000, A&AS, 142, 149

Jenkins C. R., 1998, MNRAS, 294, 69
Le Louarn M., Hubin N., 2004, MNRAS, 349, 1009
Nicholls T. W., Boreman G. D., Dainty J. C., 1995, Opt. Lett., 20, 2460
Rao C., Jiang W., Ling N., 2000, J. Mod. Opt., 47, 1111
Rao C., Jiang W., Ling N., 2002, Opt. Eng., 41, 534
Sarazin M., Roddier F., 1990, A&A, 227, 294
Tokovinin A., Le Louarn M., Viard E., Hubin N., Conan R., 2001, A&A, 378, 710
Tokovinin A., 2002, PASP, 114, 1156
Tokovinin A., 2004, PASP, 116, 941
Wilson R. W., 2002, MNRAS, 337, 103
Wilson R. W., Jenkins C. R., 1996, MNRAS, 268, 39
Wilson R. W., Bate J., Guerra J. C., Hubin N., Sarazin M., Saunter C., 2004, SPIE 5490, 748

This paper has been typeset from a TEX/LATEX file prepared by the author.